NANO LETTERS

Letter

pubs.acs.org/NanoLett

Singlet Exciton Fission-Sensitized Infrared Quantum Dot Solar Cells

Bruno Ehrler, Mark W. B. Wilson, Akshay Rao, Richard H. Friend, and Neil C. Greenham*

Cavendish Laboratory, J.J. Thomson Avenue, University of Cambridge, Cambridge CB3 0HE, United Kingdom

ABSTRACT: We demonstrate an organic/inorganic hybrid photovoltaic device architecture that uses singlet exciton fission to permit the collection of two electrons per absorbed high-energy photon while simultaneously harvesting low-energy photons. In this solar cell, infrared photons are absorbed using lead sulfide (PbS) nanocrystals. Visible photons are absorbed in pentacene to create singlet excitons, which undergo rapid exciton fission to produce pairs of triplets. Crucially, we identify that these triplet excitons can be ionized at an organic/inorganic heterointerface. We report internal quantum efficiencies exceeding 50% and power conversion efficiencies approaching 1%. These findings suggest an alternative route to circumvent the Shockley-Queisser limit on the power conversion efficiency of single-junction solar cells.

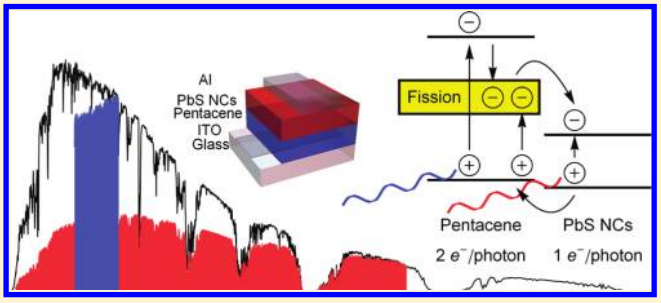

KEYWORDS: *Singlet fission, pentacene, lead sulfide, colloidal quantum dot photovoltaics, multiple carrier generation*

The desire for photovoltaic device architectures that combine reduced manufacturing costs and adequate power conversion efficiency has motivated research into candidate technologies[1] such as organic solar cells,[2,3] hybrid organic/inorganic solar cells,[4,5] and fully inorganic nanocrystal solar cells.[6] In particular, the reported efficiency of colloidal quantum dot solar cells, where the photoactive layer consists of solution-processable inorganic semiconductor nanocrystals, has recently made tremendous progress.[7] However, much of the solar energy that reaches the earth's surface lies in the infrared. Although nanocrystals that absorb in this region can be synthesized from materials such as lead sulfide (PbS),[8] much of the available energy of the visible and UV photons absorbed by such a device is lost to heat as carriers thermalize to the lowest-energy states.[9] Approaches to overcome this fundamental barrier in nanocrystal solar cells have included multiple exciton generation (MEG),[10] hot carrier collection,[11] and the use of tandem cell architectures.[12] We present an alternative route to better utilize the high-energy photons absorbed in an infrared nanocrystal solar cell.

Singlet exciton fission is a well-established process in organic semiconductors by which a photogenerated singlet exciton couples to a nearby molecule in the ground state, creating two triplet excitons.[13] In the aromatic hydrocarbon pentacene, the relaxed triplet exciton energy (0.86 eV) is less than half of the singlet energy (1.83 eV),[14,15] so that singlet fission is exothermic. Additionally, unlike common intersystem crossing, which is mediated by the spin−orbit interaction, singlet fission is spin-allowed because triplets are created as pairs that are initially coupled into a pure singlet state.[13] As a result, singlet fission in pentacene occurs extremely rapidly (~80 fs[16,17]), as we have shown in evaporated polycrystalline films.[17−19] Hence, it achieves high efficiency by kinetically out-competing alternative bulk decay channels, such as radiative recombination, multiphonon decay, or intersystem crossing, which have all been measured to have inverse rate constants >7 ns in solution.[20] Moreover, recent studies by Zhu et al. using time-resolved two-photon photoemission spectroscopy show that the photogenerated singlet predominately decays to the spin-correlated triplet pair even in the extreme case of submonolayer islands of pentacene on a C_{60} surface,[21] implying fission outcompetes the subpicosecond electron transfer at the immediately adjacent interface. Consequently, any photocurrent arising from light absorbed in the pentacene in a macroscopic photovoltaic device must stem from the dissociation of triplets created via singlet fission.

Because each of the two triplets can generate charge following dissociation at a suitable interface, the direct effect of singlet fission in a solar cell is to double the photocurrent while halving the maximum possible photovoltage. This is reflected in the low open-circuit voltage (V_{oc} < 0.5) and impressive external quantum efficiencies (EQE) of photovoltaic devices based on evaporated pentacene/fullerene bilayers (69%),[22] pentacene/phthalocyanine/fullerene trilayers (64%),[23,24] and pentacene/PTCDI blends (83%).[25] The nanosecond time scale of photocurrent generation in these devices is also consistent with the slow diffusion of triplets to the heterointerface and is incompatible with the direct dissociation of short-lived singlets.[19,24] Tantalizingly, an EQE greater than 100% was reported for a multilayer pentacene/fullerene photodetector under reverse bias, which was used to suggest that the efficiency of fission is pentacene thin-films is at least 145%.[26]

Received: December 6, 2011
Revised: January 17, 2012
Published: January 18, 2012

However, the conversion of high-energy singlets into pairs of low-energy triplets via singlet fission in these devices does not intrinsically improve the power conversion efficiency because the optical band gaps of all of the materials in these devices are similar. Instead, to enhance power conversion efficiency using singlet fission, it is necessary to combine two materials, one which generates photocurrent directly from absorbed low-energy photons, and a second which exploits fission to generate enhanced photocurrent from high-energy photons. In this respect the desired device is similar to a tandem solar cell. However, fission has the advantage that it removes the necessity of engineering a pair of current-matched cells with a transparent recombination layer, as the excitons from both materials can ideally be dissociated at the common interface. A notable disadvantage is that the energy price in dissociating the excitons must be paid twice, once for each of the two triplets. Further discussion on this topic can be found elsewhere.[1,13,27]

Here we use infrared-absorbing lead sulfide (PbS) semiconductor nanocrystals as an electron acceptor, against which the pentacene triplet exciton is dissociated. PbS nanocrystals have proved successful in expanding power conversion into the infrared and offer the opportunity to tune the band gap due to quantum confinement.[8] We tune the optical gap to 0.7 eV such that it is comparable to the pentacene triplet energy. As suggested in Figure 1, the resulting energy landscape at the

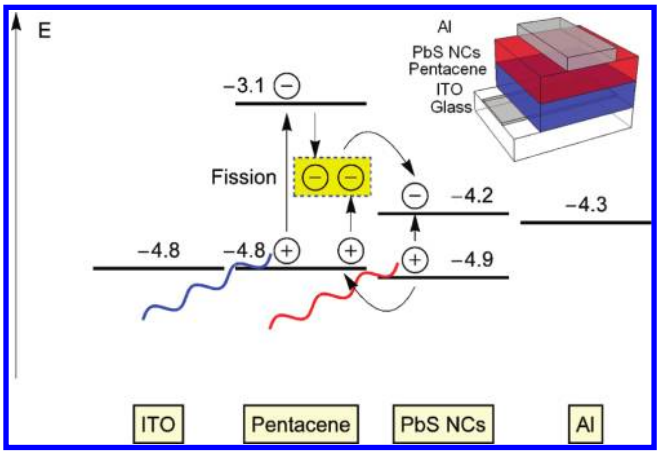

Figure 1. Device schematic and energy diagram and proposed working mechanism of the solar cells. The excited singlet state in the pentacene layer converts to two triplet states after about 80 fs. These triplets are dissociated at the pentacene/PbS nanocrystal interface. At the same time the PbS nanocrystals absorb the infrared part of the incident light. Values are from refs 38 and 43.

interface allows hole transfer from the nanocrystals to the pentacene, while also favoring ionization of the pentacene triplet excitons via electron transfer to the PbS. Hybrid, bilayer devices were designed so that the light passes through the high-energy-gap pentacene first, as pentacene is transparent to the infrared photons that are absorbed by the nanocrystals. Through this novel pairing of an organic material that undergoes fission and low-gap nanocrystals in a hybrid device architecture, it is possible to directly obtain photocurrent from infrared photons while harnessing the excess energy of visible photons to generate additional photocurrent.

Experimental Section. Chemicals: Lead(II) oxide (99.999%, PbO), oleic acid (technical grade, 90%, OA), 1-octadecene (technical grade, 90%, ODE), bis(trimethylsilyl)-sulfide (synthesis grade, TMS), hexane (anhydrous, 95%), ethanol (anhydrous, ≥99.5%), benzene-1,3-dithiol (≥99.0%, BDT), zinc acetate dihydrate (≥99.0%), methanol (dried, ≥99.9%), potassium hydroxide (99.99%, KOH), butylamine (99.5%), chloroform (anhydrous, ≥99%), and pentacene (triple-sublimed grade) were purchased from Sigma-Aldrich and used as received unless otherwise stated.

PbS Nanocrystal Synthesis. The synthesis was done entirely using air-free techniques as described elsewhere.[28] Briefly, a three-neck flask was loaded with 0.47 g of PbO dissolved in 18 g of OA and 10 g of ODE and degassed at 100 °C in vacuum for three hours. The system was flushed with nitrogen and heated to 130 °C. Separately, under a nitrogen atmosphere, 210 μL of TMS was dissolved in 4 mL of ODE (degassed in vacuum at 90 °C for 24 h) and loaded in a syringe. The content of the syringe was injected into the reaction flask and the heating was removed immediately. The system was subsequently left to cool to 35 °C. The reaction was then quenched and the nanocrystals precipitated by the injection of a mixture of 2 mL of hexane (anhydrous) in 10 mL of ethanol (anhydrous). The nanocrystals were washed twice by dissolving in hexane and precipitating with ethanol. They were then stored in octane at a concentration of 100 mg/mL under a nitrogen atmosphere.

Zinc Oxide Nanocrystal (ZnO) Synthesis. ZnO was synthesized under ambient conditions using established methods.[29] In short, 0.9788 g of zinc acetate dihydrate was dissolved in 42 mL of methanol in a three-neck flask and heated to 60 °C under air. KOH (0.469 g) was dissolved in 22 mL of methanol and dropped into the reaction flask over a period of 10 min. After a total reaction time of about 90 min, the reaction solution turns pale. At this point, the heating was switched off and the flask was cooled to room temperature by blowing nitrogen at the reaction flask. The ZnO nanocrystals were precipitated by centrifuging briefly and then redispersed in 50 mL methanol and centrifuged twice to wash off unreacted material. Finally they were dissolved in chloroform and 75 μL of butylamine was added as a stabilizing ligand. The ZnO nanocrystals form a clear solution in chloroform.

Device Fabrication. ITO-coated glass slides were purchased from Psiotec and cleaned by sequential sonication in acetone and isopropanol followed by oxygen plasma treatment. All subsequent processing was performed in a nitrogen environment (~1 ppm O_2). A 50 nm layer of pentacene was deposited onto the substrate via thermal evaporation at a rate of 0.1 Å/s under a vacuum of 2×10^{-6} mbar or better. This thickness follows the work of Kippelen et al.[30] and balances the need to maximize optical absorption while ensuring excitons can diffuse to the heterojunction where they can be dissociated to yield photocurrent. The nanocrystals were then deposited using the layer-by-layer spin coating technique described by Sargent and co-workers.[31] All layers were spun for 15 s at 1500 rpm after a 3 s wait. First, a drop of BDT in anhydrous acetonitrile (0.23 vol %) was spun onto the pentacene surface. This was found to improve the film quality, presumably because it creates a layer of molecules that preferentially attach to the nanocrystals. Excess BDT that had not attached to the surface was washed off by spinning a layer of pure acetonitrile. PbS nanocrystals were dissolved in octane and spun immediately after filtration. After the deposition of each nanocrystal layer, a further layer of BDT in acetonitrile was spun to cross-link the nanocrystals followed by a layer of acetonitrile to wash off any unreacted BDT. This procedure was reproduced until the desired thickness was reached. Aluminum top contacts were thermally evaporated at a

pressure of 3×10^{-6} mbar or better. Figure 1 shows the general structure of a typical device.

The solar cells were encapsulated by affixing a glass slide on top of the completed device using transparent epoxy and taken out of the glovebox into the ambient environment for characterization. External quantum efficiencies were measured using monochromatic light from an Oriel Cornerstone 260 monochromator. The current−voltage measurement was carried out under an Oriel 92250A solar simulator with a Keithley 2636A source measure unit. The incident power was corrected for the spectral mismatch of the lamp used in the solar simulator over the spectral region from 375 to 1045 nm. We note that the solar cells tested here absorb light up to 1770 nm hence the correction for the spectral mismatch is not completely accurate. However, even in a worst-case scenario, this discrepancy is not expected to change the result by more than 4%.

Optical Properties of PbS, ZnO, and Pentacene. To perform variable-angle spectroscopic ellipsometry, films of PbS nanocrystals and ZnO nanocrystals were spin-coated on a silicon/silicon dioxide wafer and measured in reflection while the pentacene was evaporated onto a quartz-glass substrate and measured in transmission. The thicknesses were estimated using an atomic force microscope. The change in polarization of the incident light was measured with a J.A. Woollam variable-angle spectroscopic ellipsometer. The data were fitted with a Cauchy model in the transparent region to find the thickness and then by a point-by-point model to extract the refractive index n and the extinction coefficient k over the whole wavelength range. The fit for the PbS nanocrystals was less accurate due to a lack of a transparent region so the extinction coefficient was calculated directly from the measured absorbance. The refractive index and the extinction coefficient for lead sulfide and zinc oxide nanocrystals as well as evaporated pentacene are shown in Figure 2. The extinction

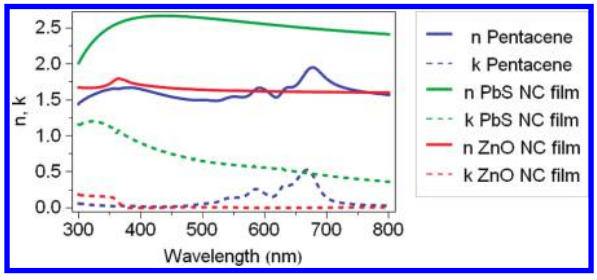

Figure 2. Refractive index (n) and extinction coefficient (k) of the pentacene and lead sulfide and zinc oxide nanocrystals determined by variable-angle spectroscopic ellipsometry.

coefficient of ZnO depends heavily on the crystallinity. Much larger values are reported for monocrystalline ZnO but our values are in good agreement with data reported for ZnO nanocrystals.[32] The optical field in the devices was modeled from the ellipsometry data using established procedures.[33−35] With the extinction coefficient known, the fraction of light absorbed in each layer could be calculated as a function of the wavelength. The IQE was then determined by dividing the measured external quantum efficiency by the sum of the absorbed light fractions of the PbS layer and the pentacene layer.

Results. Figure 3 shows the external quantum efficiency (EQE) of a hybrid bilayer solar cell with 50 nm layers of both

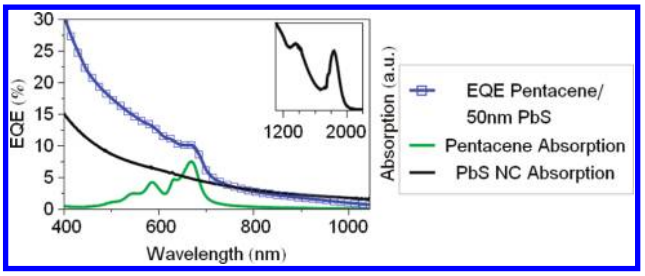

Figure 3. External quantum efficiency of a device with 50 nm layers of both pentacene and PbS nanocrystals (blue, □) in comparison with the absorption of pure pentacene (green) and nanocrystal films (black). The inset shows the absorption onset of the nanocrystals in the infrared region.

pentacene and PbS nanocrystals. The shape of the EQE spectrum follows the absorption of the nanocrystals but shows a pronounced peak at 680 nm, implying an additional contribution from the absorption of pentacene. This shows that photocurrent is generated from both layers at the same time. As described above, photocurrent from pentacene stems from the ionization of pairs of triplets created by rapid singlet fission. Hence, the pentacene-sensitized, IR-absorbing solar cell presented here is the realization of a device that simultaneously absorbs low-energy photons and harnesses the excess energy of high-energy photons via singlet fission.

The observation of photocurrent from dissociated triplet excitons is significant. This is because Förster transfer between the triplet exciton in pentacene and the nanocrystals is forbidden,[36] hence the ionization of triplets at this interface would proceed through direct electron transfer to the conduction band of the nanocrystals. Although the spectral signature of pentacene is evident in the EQE of devices made with low-gap (0.7 eV) nanocrystals, it was not detected in a control experiment using PbS nanocrystals with an optical gap of 1.3 eV. This lack of photocurrent with larger-bandgap nanocrystals has been reported previously[37] and was attributed to an undesirable interfacial energy-level shift. Instead, we propose that lack of photocurrent when using high-gap nanocrystals results because the conduction band of the acceptor (PbS nanocrystals[38]) is not low enough to ionize the triplet. We note that such a low conduction band energy would not appear necessary if photocurrent was generated via the direct dissociation of the high-energy singlet exciton in pentacene, since it has been demonstrated that an energy offset of a few hundred millielectronvolts can be sufficient to dissociate singlets in other systems.[39,40] Instead this result is consistent with the ionization of triplets produced via rapid, efficient singlet fission.[16−19,26]

The IQE calculated from the optical modeling in the device with a thin (50 nm) PbS layer is presented in Figure 4a. We find a small enhancement of the IQE in the region of the pentacene absorption. This is consistent with an increase in the yield of charges per photon due to exciton fission, but could also be explained without invoking exciton fission by a relative difference in the charge generation efficiencies of the individual layers.

Although the device with a thin layer of PbS nanocrystals most clearly showed the contribution from pentacene, the overall efficiency could be improved by increasing the thickness of the PbS layer. Figure 4b presents the measured EQE and calculated IQE of a pentacene-sensitized device with a 130 nm PbS nanocrystal layer. This thickness was chosen using the

dx.doi.org/10.1021/nl204297u | *Nano Lett.* 2012, 12, 1053−1057

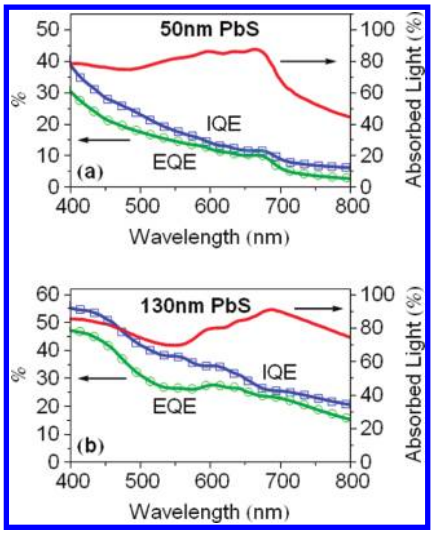

Figure 4. External (green, ○) and internal quantum efficiencies (blue, □) for (a) the 50 nm (thin) and (b) the 130 nm (thick) PbS layer device. Both devices have a 50 nm layer of pentacene. The red curve represents the fraction of the incident energy absorbed in the nanocrystal and pentacene layers.

optical modeling to predict the device architecture that would improve overall absorption while preserving a strong contribution from the pentacene in the EQE spectrum. We observe a substantial increase in the EQE of the device across the measured spectrum, which we attribute to the enhanced absorption as well as superior electrical properties arising from improved film formation. Additionally, while the relative contribution to the EQE from pentacene is decreased when compared to the thin device, a spectral signature consistent with the modeled two-layer absorption spectrum remains evident. However, the lack of an enhancement in the IQE in the region of strong pentacene absorption suggests the efficiency of collection of charges from triplet excitons in the pentacene is lower than that from nanoparticle excitons in the thicker cell. Further optimization is thus required to take full advantage of the additional excited states generated through the singlet fission process.

To further improve the performance of the device, we investigated the effect of adding a layer of zinc oxide (ZnO) nanocrystals between the PbS nanocrystals and the metallic top contact to improve charge extraction[41] and to serve as an optical spacer.[42] The thickness of this layer (100 nm) was again determined using optical modeling to beneficially redistribute the optical field in the device for absorption in the pentacene. As shown in Figure 5, the addition of the ZnO layer increases the power conversion efficiencies under AM 1.5 solar illumination by a factor of 5, leading to a PCE of 0.85%. The device parameters are listed in Table 1. We attribute the majority of the improvement in cell performance to an increase in charge extraction and the hole-blocking nature of the ZnO, since our modeling suggests that the incorporation of 100 nm ZnO only increases the overall light intensity absorbed by the cell by 5%.[41] We emphasize that the 50 nm pentacene layer is still present, suggesting that it is compatible with efficient hole extraction. These preliminary results show the potential for further performance improvements via the joint optimization of optical and electrical performance through the careful tuning of the layer thicknesses.

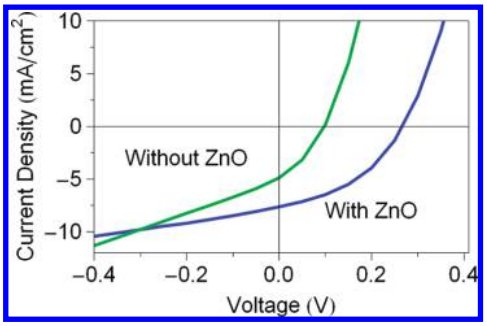

Figure 5. The effect of a ZnO nanoparticle layer on device performance under AM1.5G illumination at 1 sun.

Table 1. Device Parameters for the Solar Cells with a 130 nm Thick PbS Layer with and without a Layer of ZnO Nanocrystals (See Text)[a]

	no ZnO	100 nm ZnO nanocrystals
J_{SC} (mA/cm^2)	4.86	7.61
V_{OC} (V)	0.10	0.27
FF	33%	41%
PCE	0.16%	0.85%

[a]The parameters are measured under AM1.5G illumination at 1 sun. The spectral mismatch was taken into account as described in the Experimental Section.

Conclusions. We have successfully fabricated a solar cell that simultaneously harvests photocurrent from triplet excitons created by singlet fission in pentacene and low energy photos absorbed in lead sulfide nanocrystals without requiring a tandem geometry. We have demonstrated that triplet excitons can be dissociated at an organic−inorganic interface. Preliminary device optimization yields solar cells with power conversion efficiencies approaching 1% under one sun illumination and internal quantum efficiencies exceeding 50%. A sizable parameter space remains in which to further improve device performance and move toward the goal of achieving quantum efficiencies greater than 100%.

AUTHOR INFORMATION

Corresponding Author

*E-mail: ncg11@cam.ac.uk.

Notes

The authors declare no competing financial interest.

ACKNOWLEDGMENTS

B.E. thanks Dr. Brian Walker for useful discussions and the EPSRC SUPERGEN Excitonic Solar Cells Consortium for funding. M.W.B.W. and A.R. thank the Cambridge Commonwealth Trust for funding and A.R thanks Corpus Christi College for a research fellowship. This project was supported by the Engineering and Physical Sciences Research Council.

REFERENCES

(1) Lunt, R. R.; Osedach, T. P.; Brown, P. R.; Rowehl, J. A.; Bulović, V. *Adv. Mater.* **2011**, *23*, 5712−5727.
(2) McNeill, C. R.; Greenham, N. C. *Adv. Mater.* **2009**, *21*, 3840−3850.
(3) Brabec, C. J.; Gowrisanker, S.; Halls, J. J. M.; Laird, D.; Jia, S.; Williams, S. P. *Adv. Mater.* **2010**, *22*, 3839−56.
(4) Greenham, N. C.; Peng, X.; Alivisatos, A. P. *Phys. Rev. B* **1996**, *54*, 17628−17637.

(5) Talapin, D. V.; Lee, J.-S.; Kovalenko, M. V.; Shevchenko, E. V. *Chem. Rev.* **2010**, *110*, 389−458.
(6) Gur, I.; Fromer, N. A.; Geier, M. L.; Alivisatos, A. P. *Science* **2005**, *310*, 462−5.
(7) Kramer, I. J.; Sargent, E. H. *ACS Nano* **2011**, *5* (11), 8506−8514.
(8) Tang, J.; Sargent, E. H. *Adv. Mater.* **2011**, *23*, 12−29.
(9) Shockley, W.; Queisser, H. J. *J. Appl. Phys.* **1961**, *32*, 510−519.
(10) Nozik, A. J. *Nano Lett.* **2010**, *10*, 2735−41.
(11) Tisdale, W. A.; Williams, K. J.; Timp, B. A.; Norris, D. J.; Aydil, E. S.; Zhu, X.-Y. *Science* **2010**, *328*, 1543−7.
(12) Wang, X.; Koleilat, G. I.; Tang, J.; Liu, H.; Kramer, I. J.; Debnath, R.; Brzozowski, L.; Barkhouse, D. A. R.; Levina, L.; Hoogland, S.; Sargent, E. H. *Nat. Photonics* **2011**, *5*, 480−484.
(13) Smith, M. B.; Michl, J. *Chem. Rev.* **2010**, *110*, 6891−6936.
(14) Rei Vilar, M.; Heyman, M.; Schott, M. *Chem. Phys. Lett.* **1983**, *94*, 522−526.
(15) Burgos, J.; Pope, M.; Swenberg, C. E.; Alfano, R. R. *Phys. Status Solidi B* **1977**, *83*, 249−256.
(16) Jundt, C.; Klein, G.; Sipp, B.; Le Moigne, J.; Joucla, M.; Villaeys, A. A. *Chem. Phys. Lett.* **1995**, *241*, 84−88.
(17) Wilson, M. W. B.; Rao, A.; Clark, J.; Kumar, R. S. S.; Brida, D.; Cerullo, G.; Friend, R. H. *J. Am. Chem. Soc.* **2011**, *133*, 11830−3.
(18) Rao, A.; Wilson, M. W. B.; Albert-Seifried, S.; Di Pietro, R.; Friend, R. H. *Phys. Rev. B* **2011**, *84*, 195411.
(19) Rao, A.; Wilson, M. W. B.; Hodgkiss, J. M.; Albert-Seifried, S.; Bässler, H.; Friend, R. H. *J. Am. Chem. Soc.* **2010**, *132*, 12698−703.
(20) Nijegorodov, N.; Ramachandran, V.; Winkoun, D. P. *Spectrochim. Acta, Part A* **1997**, *53*, 1813−1824.
(21) Chan, W.-L.; Ligges, M.; Jailaubekov, A.; Kaake, L.; Miaja-Avila, L.; Zhu, X.-Y. *Science* **2011**, *334*, 1541−1545.
(22) Yoo, S.; Potscavage, W. J. Jr.; Domercq, B.; Han, S.-H.; Li, T.-D.; Jones, S. C.; Szoszkiewicz, R.; Levi, D.; Riedo, E.; Marder, S. R.; Kippelen, B. *Solid-State Electron.* **2007**, *51*, 1367−1375.
(23) Kinoshita, Y.; Hasobe, T.; Murata, H. *Appl. Phys. Lett.* **2007**, *91*, 083518.
(24) Hong, Z. R.; Lessmann, R.; Maennig, B.; Huang, Q.; Harada, K.; Riede, M.; Leo, K. *J. Appl. Phys.* **2009**, *106*, 064511.
(25) Pandey, A. K.; Dabos-Seignon, S.; Nunzi, J.-M. *Appl. Phys. Lett.* **2006**, *89*, 113506.
(26) Lee, J.; Jadhav, P. J.; Baldo, M. A. *Appl. Phys. Lett.* **2009**, *95*, 033301.
(27) Jadhav, P. J.; Mohanty, A.; Sussman, J. M.; Lee, J.; Baldo, M. A. *Nano Lett.* **2011**, *11*, 1495−8.
(28) Gao, J.; Luther, J. M.; Semonin, O. E.; Ellingson, R. J.; Nozik, A. J.; Beard, M. C. *Nano Lett.* **2011**, *11*, 1002−8.
(29) Pacholski, C.; Kornowski, A.; Weller, H. *Angew. Chem., Int. Ed.* **2002**, *41*, 1188−91.
(30) Yoo, S.; Domercq, B.; Kippelen, B. *Appl. Phys. Lett.* **2004**, *85*, 5427.
(31) Pattantyus-Abraham, A. G.; Kramer, I. J.; Barkhouse, D. A. R.; Wang, X.; Konstantatos, G.; Debnath, R.; Levina, L.; Raabe, I.; Nazeeruddin, M. K.; Grätzel, M.; Sargent, E. H. *ACS Nano* **2010**, *4*, 3374−80.
(32) Lakhwani, G.; Roijmans, R. F. H.; Kronemeijer, A. J.; Gilot, J.; Janssen, R. A. J.; Meskers, S. C. J. *J. Phys. Chem. C* **2010**, *114*, 14804−14810.
(33) Pettersson, L. A. A.; Roman, L. S.; Inganäs, O. *J. Appl. Phys.* **1999**, *86*, 487.
(34) Peumans, P.; Yakimov, A.; Forrest, S. R. *J. Appl. Phys.* **2003**, *93*, 3693.
(35) Burkhard, G. F.; Hoke, E. T.; McGehee, M. D. *Adv. Mater.* **2010**, *22*, 3293−7.
(36) Köhler, A.; Bässler, H. *Mater. Sci. Eng. R* **2009**, *66*, 71−109.
(37) Dissanayake, D. M. N. M.; Hatton, R. A.; Lutz, T.; Curry, R. J.; Silva, S. R. P. *Nanotechnology* **2009**, *20*, 195205.
(38) Jasieniak, J.; Califano, M.; Watkins, S. E. *ACS Nano* **2011**, *5*, 5888−902.
(39) Veldman, D.; Meskers, S. C. J.; Janssen, R. a. J. *Adv. Funct. Mater.* **2009**, *19*, 1939−1948.
(40) Gong, X.; Tong, M.; Brunetti, F. G.; Seo, J.; Sun, Y.; Moses, D.; Wudl, F.; Heeger, A. J. *Adv. Mater.* **2011**, *23*, 2272−7.
(41) Hau, S. K.; Yip, H.-L.; Baek, N. S.; Zou, J.; O'Malley, K.; Jen, A. K.-Y. *Appl. Phys. Lett.* **2008**, *92*, 253301.
(42) Yang, T.; Cai, W.; Qin, D.; Wang, E.; Lan, L.; Gong, X.; Peng, J.; Cao, Y. *J. Phys. Chem. C* **2010**, *114*, 6849−6853.
(43) Griffith, O. L.; Anthony, J. E.; Jones, A. G.; Lichtenberger, D. L. *J. Am. Chem. Soc.* **2010**, *132*, 580−6.